Evaluation of the atmospheric transport model NIRE-CTM-96 by using measured radon-222 concentrations

By SHOICHI TAGUCHI[1]*, TAKAO IIDA[2] and JUN MORIIZUMI[2], [1]*National Institute of Advanced Industrial Science and Technology, AIST Tsukuba West, 16-1 Onogawa, Tsukuba, Ibaraki, 305-8569, Japan;* [2]*Graduate School of Engineering, Nagoya University, Furo-cho, Chikusa-ku, Nagoya, 464-8603, Japan*

ABSTRACT

An atmospheric transport model, NIRE-CTM-96, was evaluated by using measured radon-222 concentrations. The model has 2.5×2.5 degree horizontal resolution and 15 vertical levels. Assimilated global meteorological data for 1990–1996 from the European Centre for Medium Range Weather Forecasts were used to drive the model. We used an emanation rate of radon-222 of 1 atom $cm^{-2} s^{-1}$ over mostly ice-free land. Simulated concentrations were compared with measured concentrations for 22 sites worldwide including 10 stations in China. Simulated annual mean concentrations for Freiburg, Germany, and Socorro, New Mexico, and for four stations in northern China were consistent with the measured concentrations. Simulated daily concentrations for Ogasawara-Hahajima, Japan, correlated well with the measured concentrations. Simulated upper tropospheric concentrations for Moffet Field, California, demonstrated the cross-Pacific transport from central Eurasia and India–Indochina area. Simulated concentrations for two stations in southern China were almost half of the measured concentrations. Mixing layer depth in the model was consistent with other estimates which indicates higher emanation rate there. Simulated concentrations for the South Indian Ocean and the Antarctic during summer were significantly lower than the measured concentrations; this difference was accounted for when emanation from the ocean at a rate of 0.01 atom $cm^{-2} s^{-1}$ was included in the model. The model failed to simulate amplitudes of high-concentration events at Mauna Loa. These high-concentration events were possibly a result of filament-like horizontal structure or laminated vertical structure. The vertical as well as horizontal resolution of the model were supposed to be insufficient to reproduce these fine structures.

1. Introduction

Regional budget of carbon dioxide and other global warming gases is an issue involving biogeochemistry as well as international political and economical negotiations. A number of atmospheric transport models to represent global distributions of minor constituents in the atmosphere

have been developed as a tool to infer the source strengths of constituents in accord with the accumulation of monitoring data. A careful calibration and validation of a transport model is required to make a reliable estimate of the source and sink of gases. Performance of a transport model is limited partly by the quality of winds for transport calculations in the model and partly by the representation of the transport and diffusion processes, as well as the spatial and temporal resolutions. The goal of the present paper was to evaluate the perform-

* Corresponding author.
e-mail: s.taguchi@aist.go.jp

ance of an atmospheric transport model, NIRE-CTM-96, and to determine possible deficiencies and limitations of the model. The evaluation was done by comparing the radon-222 (^{222}Rn) concentrations simulated by the model and those measured worldwide.

Radon-222 is a fission product of radium-226 contained in soil. ^{222}Rn has poor solubility in water, and is chemically inert. Due to its short half-life of 3.82 d and its relatively homogeneous emission over land, ^{222}Rn has been used as a tag for air parcels recently mixed with planetary boundary layer air. From the fallout rate of Pb-210, which is a fission product of ^{222}Rn, Turekian et al. (1977) estimated that the global emanation rate of ^{222}Rn is 1.2 atom cm^{-2} s^{-1}. Using an updated worldwide database for radium content combined with a ^{222}Rn flux model, Schery and Wasiolek (1998) estimated an global emanation rate of 34 ± 9 mBq m^{-2} s^{-1} (1 atom cm^{-2} s^{-1} = 21 mBq m^{-2} s^{-1}). Most of the uncertainty in the estimation of ^{222}Rn emanation rate is due to lack of knowledge about, for example, soil grain size, soil wetness, and the abundance of radium-226 in the soil.

Various studies have measured ^{222}Rn concentrations. Outdoor ^{222}Rn concentrations extensively studied in the 1950s by the US Navy were summarized by Lockhart (1964), and those in the 1960s and 1970s in India by Mishra et al. (1980). Long-term measurements over the South Indian Ocean and the Antarctic were reported by Lambert et al. (1970). Some of the studies prior to 1980 were summarized by Gesell (1983). Concentrations over China in the 1990s were reported by Jin et al. (1998).

Radon-222 is widely used to evaluate vertical transport and long-range transport in chemical transport models (Heimann and Keeling, 1989; Jacob and Prather, 1990; Feichter and Crutzen, 1990, Genthon and Armengaud, 1995; Ramonet et al., 1996; Mahowald et al, 1997; Brasseur et al., 1998; Dentener et al., 1999). Although an emanation rate of 1 atom cm^{-2} s^{-1} explains the atmospheric concentration over most of the world, there are exceptions, such as the middle Pacific troposphere. Jacob et al. (1997) showed that concentrations at 300 hPa over Mauna Loa (MLO) could not be simulated with any transport model available at that time. Ramonet et al. (1996) compared an atmospheric transport model (TM2)

with ^{222}Rn observations made during the TROPOZ-II campaign, which is a campaign conducted by the National Oceanic and Atmospheric Administration (NOAA) using aircraft to measure ^{222}Rn. Based on the vertical profiles in TROPOZ-II, they concluded that vertical transport modeled in the TM2 was excessive. By using ^{222}Rn concentration measured at Moffet Field (Kritz et al., 1998), Stockwell et al. (1998) validated a transport model developed at the University of Cambridge. They tested two horizontal resolutions (7.5 × 7.5 and 2.8 × 2.8) with and without convective transport, and found that model-data agreement was degraded if the model resolution was decreased. Dentener et al. (1999) used on-line (ECHAM) and off-line (TM3) global models to simulate ^{222}Rn concentrations and discussed possible high emanation in 80°–110°E, 0–40°N (East Asia) as previously suggested by Mahowald and Kashibhatla (personal communication, 1995) and by Kaminski (personal communication, 1997).

The goal of the current study was to determine possible deficiencies of the NIRE-CTM-96 model by comparing simulated and measured ^{222}Rn concentrations for 22 sites worldwide from eight inland stations, six coastal stations, and eight remote stations. For comparison with published results for other models, in the simulations we assumed that the emanation rate used at the WMO Workshop was accurate. In our comparison, recent measurements for east Asia were used to test the hypothesis of high emanation rate at East Asia. Our comparison includes time-resolved concentrations at Ogasawara-Hahajima and Mauna Loa and vertical profiles at Moffet field. Finally, we determined possible deficiencies in the transport model and also possible corrections to the estimated emanation rate of ^{222}Rn.

2. Atmospheric transport model, NIRE-CTM-96

A global atmospheric transport model developed at the former National Institute for Resources and Environment (NIRE-CTM-96, Taguchi et al., 2002) was used in this work and is a modified version of NIRE-CTM-93 (Taguchi et al., 1996). [Both NIRE-CTM-96 and NIRE-CTM-93 were compared with other models in an international model intercomparison project

(TransCom) of the International Geosphere Biosphere Programme (IGBP); Phase One (Law et al., 1996) and Phase Two (Denning et al., 1999)]. The model NIRE-CTM-96 has 2.5-degree horizontal resolution and has 15 vertical levels. The lowest two layers are sigma (0.99, 0.925) and the highest nine layers are pressure (300, 250, 200, 150, 100, 70, 50, 30, 10 hPa). The middle four layers are a mixture of pressure and sigma (hybrid). Advection is calculated by using a semi-Lagrangian scheme. In the simulations, ^{222}Rn concentrations were calculated for 6-h periods.

In the simulations, a complete vertical mixing was applied below the top of the mixed layer so that concentrations in the mixed layer were homogeneous. The height of the mixed layer was estimated for each 6-h interval by using the bulk Richardson number (Troen and Mahrt, 1986). Temperature at 2 m above surface was used for bottom air temperature for calculating the bulk Richardson number. A lowest layer was always included in the mixed layer regardless of the height of the mixed layer. The number of levels in the mixed layer varies from time to time and at horizontal locations. The lowest possible mixed layer height was the 0.9575 sigma level, because mixed layer height in the model was specified at the center of the model level, thus making the minimum thickness of the mixed layer at 42.5 hPa (about 300 m) for a surface pressure of 1000 hPa. Also note that we do not distinguish a thick layer mixed by deep moist convections from a boundary layer mixed by dry convections. A disputable feature of the current method is a deep mixed layer over the large-scale mountains resulted from high surface air temperature.

A major improvement of NIRE-CTM-96 is the reduced stratosphere–troposphere exchange rate in terms of turnover time (1.8 yr), which was too fast in the NIRE-CTM-93 (0.5 yr). The reduction of turnover time was achieved by the change in interpolation scheme at around tropopause specified with the thermal definitions (Hoinka, 1998). We adopted 13 K km^{-1} as a critical lapse rate of potential temperature. At the departure point in the semi-Lagrangian scheme in the model, linear interpolation was used as a default for estimating tracer concentration. At the outside of the tropics, north of 30°N and south of 30°S, if the departure point was located between levels where the tropopause was detected, the value on the grid nearest

to the departure point was used without any interpolation. In the tropics, when a departure point was located between levels where the tropopause was detected, the value at the horizontal location of the departure point was estimated using linear interpolation on the single nearest level, above or below the departure point, and was used for concentration at the departure point without interpolation between levels.

Although the semi-Lagrangian scheme used in the model guarantees positive concentration, the total loading of tracer in the model atmosphere is not necessarily conserved. Therefore, in our simulation, we used a mass fixer described by Taguchi (1996) to maintain a constant total mass of tracer.

Meteorological data used in this model are assimilated data obtained from the European Centre for Medium Range Weather Forecasts (ECMWF). In our simulations, we used the following data collected for a 7-yr period, from January 1990 to December 1996: pressure at the surface, temperature at 2 m from the surface, and temperature and wind at 15 pressure levels between 1000 and 10 hPa. Data were given at 6-h intervals (0, 6, 12, 18 UTC).

3. Mean seasonal cycle for the land emanations

In our simulations for the evaluation of this model, we used the emission of 1 atom cm^{-2} s^{-1} for all land areas between 60°S and 60°N, and 0.5 atom cm^{-2} s^{-1} for land areas between 60°N and 70°N (excluding Greenland). The emission is identical to that used at the World Climate Research Program (WCRP) Workshop (Jacob et al., 1997), except for oceanic emissions. The model simulated 7-yr periods beginning 1 January 1990, using an initial condition of zero ^{222}Rn concentration. In this evaluation, we analyzed the last 6-yr results. To evaluate possible sources for the discrepancies between the simulated and measured data, we did a supplementary set of simulations in which we used an emanation rate of 0.01 atom cm^{-2} s^{-1} over the ocean between 60°N and 60°S.

3.1. Simulated and measured ^{222}Rn concentrations at different sites worldwide

The simulated ^{222}Rn concentrations were compared with a standard data set reported in the

literature. Figure 1 shows the simulated and measured concentrations at sites listed in Fig. 3 of Brasseur et al. (1998), except Kirov and Soccoro. Note that model concentrations were available at 6-hr intervals, and thus the local time differed among the sites if afternoon surface concentrations were used for comparison.

(a) Freiburg (48.0°N, 7.8°E). Concentrations at the surface were measured by Bundesamt für Zivilschutz, Institut für Radioaktivität, Freiburg. We adopted the mean surface values for 1993 reported by Dentener et al. (1999). In our simulation, first, a daily average concentration was calculated. Then, the mean and quartiles of monthly
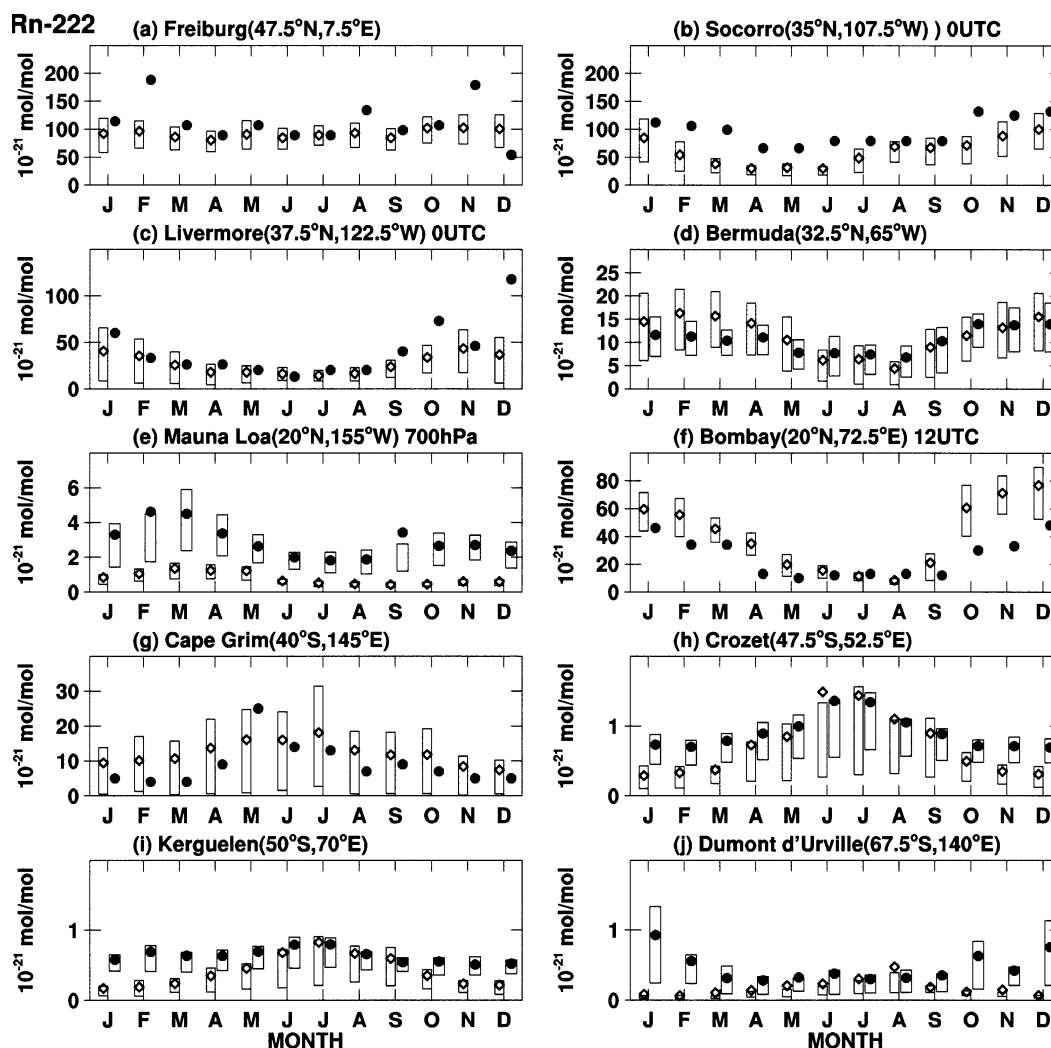

Fig. 1. [222]Rn concentrations measured (closed circles) and simulated by using the global atmospheric transport model NIRE-CTM-96 (open circles). Mean values are shown. Box indicates quartile of daily average of concentration simulated for a 6-yr period, between 1991 and 1996. If specific time is used for model results, time is shown in universal time coordinates (UTC). Sampling locations in the model are also shown. Concentrations at lowest model levels were used for sites except Mauna Loa, where those at 700 hPa were used. Sites of measured concentrations and details of the data source are given in the text.

concentrations for a 6-yr period were calculated. Simulated mean concentrations for the 6-yr period were consistent with measured concentrations, except for February and November. No significant difference was observed for simulated mean and quartiles for February and November 1993. Causes of these discrepancies between the simulated and measured concentrations at inland stations and remote stations in the southern Hemisphere will be discussed at the end of this section.

(b) Socorro, New Mexico (34.1°N, 106.9°W). Wilkening (1959) reported surface concentrations for 6-yr monitoring beginning from 1951. We adopted the monthly mean surface values for 15LST reported by Jacob and Prather (1990). The simulated mean concentrations for Socorro were consistent with the measured concentrations, except in the spring. Model concentrations were taken at 17LST (0 UTC).

(c) Livermore, California (37.7°N, 121.8°W). Lindken (1966) reported surface concentrations between May 1965 and August 1966. We adopted the afternoon surface values reported by Gesell (1983). Model concentrations were taken at 16LST (0 UTC). Our model underestimated the concentrations for December. Simulated concentrations at coastal sites, such as Livermore, are sensitive to relative locations between the grid where the site is represented and the grids at which emissions are given. The relative locations were determined automaticaly by the setting of the mesh in the simulation.

(d) Bermuda (32.3°N, 64.7°W). The Environmental Measurement Laboratory, Department of Energy (EML/DOE, USA) measured surface concentration every half-hour. We adopted data (1993–1996) available from the DOE website (http://www.doe.gov). Because local meteorological data were not available, we did not select specific data by wind direction, such as Dentener et al. (1999) did for Bermuda. The mean and quartiles of concentrations calculated by our model compared well with the measured concentrations by EML/DOE, except those for spring. Those for spring were overestimated, similar to the overestimation reported by Dentener et al. (1999).

(e) Mauna Loa, Hawaii (19.5°N, 155.6°W, 3400 m). EML measured the concentration near the top of a mountain (1993–1996). Again, we obtained the data from the DOE website and considered the data as middle tropospheric concentrations rather than surface concentrations. In our calculations of mean and quartiles, we only used concentrations measured during the night from 0 am to 7 am to minimize local source of ^{222}Rn at Mauna Loa, as suggested by Dentener et al. (1999). The measured mean values for February and September exceed the quartiles. This indicates that some short-term extreme peaks increased the mean value for that month. Although our model significantly underestimated the measured concentrations, it well reproduced the concentrations calculated by TM3-FG (Dentener et al., 1999). Causes for the discrepancies between the simulated and measured concentrations will be discussed in Section 6.

(f) Bombay (18.9°N, 72.8°E). Surface concentrations were measured during 1966–1976 by Mishra et al. (1980). We used the afternoon surface values reported by Gesell (1983). Model concentrations were taken at 17LST (12 UTC). Seasonal variations estimated by our model were consistent with observations. However, our model overestimated the concentrations from October to December. No further discussion was made on this site because the site was located on the coast.

(g) Cape Grim (40.7°S, 144.7°E). Surface concentrations were measured from July 1990 to June 1991 by Stewart Whittlestone (personal communication, 1995). We used the surface values used by Mahowald et al. (1997). The simulated concentrations were higher than the measured concentrations. No further discussion was made on this site because the site was located near the coast.

(h) Crozet (46.4°S, 51.9°E), (i) Kerguelen (49.4°S, 70.3°E), (j) Dumont d'Urville (66.7°S, 140.0°E). Concentrations were measured by the French Centre de Faibles Radioactivités with a time resolution of 1–2 h (Lambert et al., 1970). The data were kindly supplied by Y. J. Balkanski (personal communication, 1995) and contain following periods: Crozet, 1968–1994; Kerguelen, 1967–1992; Dumont d'Urville, 1967–1981. At these three sites, simulated concentrations for

winter compared well with the measured concentrations. However, our model significantly underestimated the concentrations for summer. A possible effect of emissions from the ocean will be discussed in the next subsection.

3.2. Possible causes for the discrepancies between simulated and measured concentrations

At this section, we only discuss two effects that possibly explain the discrepancies between the simulated and measured concentrations, one is the mixed layer at inland stations and the second is the emission from the ocean. Concentrations at inland stations were determined by the accumulation of ^{222}Rn in stable layers and ventilations due to entrainment of free tropospheric air during the expansion of mixed layer. The minimum mixed layer height in the current model was about 300 m, which might be higher than the actual stable layers. This limitation caused by vertical spacing of the model grid is a possible explanation for the underestimation of the concentration in February and November at Freiburg. At Freiburg, although the concentrations simulated by using our model were consistently lower than those by using TM3-FG or ECHAM (Dentener et al., 1999), our results agreed well with the measured concentrations.

Ventilation of air in surface boundary layer might be evaluated by using the daily highest mixed layer because mixed layer was usually a single lowest layer at night. Daily maximum thickness of mixed layer at two inland stations, Freiburg and Socorro, are shown in Fig. 2. Mixed layer thickness was defined at 6-hr intervals and maximum thickness occurred usually in the afternoon, local time. Mean and standard deviations were estimated for each month from 1990 to 1996. In our model, we denote the daily maximum mixed layer thickness as maximum mixing depth (MMD), according to Gamo et al. (1993).

Seasonal cycles of MMD at Freiburg and Socorro are interpreted as a thin mixed layer due to stable layers formed by radiative cooling of the ground in winter and the thick mixed layer created by dry and moist convective activity in summer. Differences in MMD for these two locations are due to differences in climate and altitudes of the stations, 500 m (Freiburg) and 2000 m (Socorro). The MMD at Socorro was estimated to be 8 km in the model in June, due to the very high temperature at 2 m above the ground. Simulated concentrations were lower than the observations during February to July, which indicates the depth of mixed layer in the model might be thicker than the actual mixed layer. Although a mixed layer extending up to 8 km was observed over Scottsbluff, Nebraska (Moor et al., 1973), further improvement in the estimate of mixed layer may be required in the model to fit the simulations with the observations, especially over high terrains.

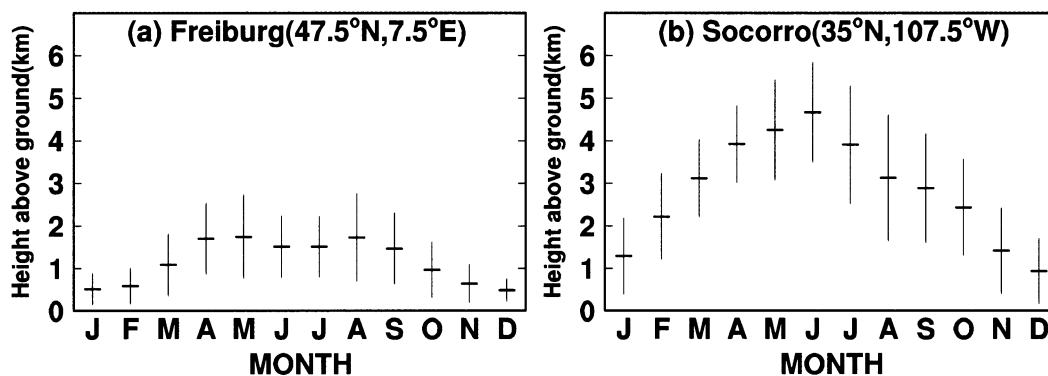### Daily Maximum Thickness of Mixed Layer(km) (1990-1996)

Fig. 2. Daily maximum thickness of well-mixed layer in the model at Freiburg (a) and Socorro (b). Daily maximum mixed layer thickness was calculated every day and was averaged over 7 yr (horizontal bar). Vertical bar indicates standard deviation of daily maximum thickness.

At Crozet and Kerguelen, concentrations from oceanic sources (0.01 atom cm^{-2} s^{-1}) were estimated as about 1×10^{-21} mol mol^{-1}. At Dumont d'Urville, these concentrations were about 0.1×10^{-21} mol mol^{-1} in our supplementary simulations in which the southern edge of the ocean emission was 60°S. Detailed representation of the location of the edge of sea ice and the conditions of ice around the site might be required for accurate simulations of surface radon at Dumont d'Urville. In contrast to our model, TM3-FG overestimated the ^{222}Rn concentrations at Kerguelen and Crozet even though emissions from the ocean were not included in the TM3-FG (Dentener et al., 1999). Our model reproduced (not shown) the summer radonic storm shown in Fig. 7 in Dentener et al. (1999). Because emanation from ocean accounted for the discrepancies, we do not regard the discrepancies at Crozet, Kerguelen, and Dumont d'Urville as shortcomings of the atmospheric transport model (NIRE-CTM-96) that we used.

4. China

Emanation rate at China is of concern due to its high rate. Jin et al. (1998) reported annual mean surface ^{222}Rn concentrations at 10 sites in China. Observations were made for two separate 1-yr periods, November 1988 to November 1989 and April 1991 to April 1992. Figure 3 shows locations of the monitoring sites in China. Intersections in the mesh indicate the locations in the model grid at which the ^{222}Rn concentrations were calculated by using the atmospheric transport model NIRE-CTM-96. Concentrations at the model gridpoint nearest the monitoring site (x) were used for simulated concentrations. No fractional land was considered at the coast, which means the emission is either all (indicated by 1 in the figure) or nothing at the individual gridpoint.

Figure 4 is the same as Fig. 1 except that it is for measurements in China. Horizontal lines are the annual mean concentrations reported by Jin et al. (1998). Inland stations (monitoring stations far from coast) are shown in the left column, ordered from north to south. One additional inland station (Changchun) is shown in the top panel in the right column. Simulated concentrations were about $(100$–$150) \times 10^{-21}$ mol mol^{-1},
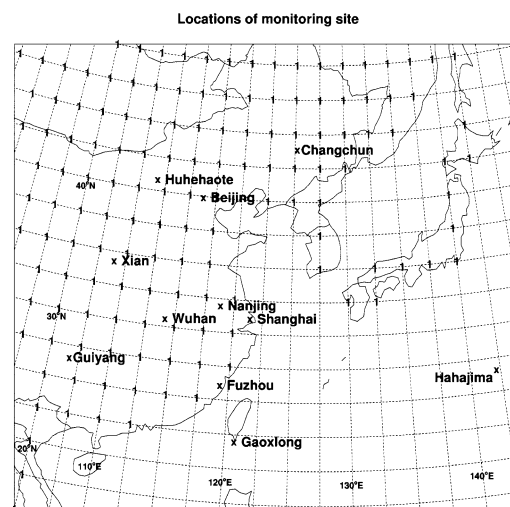

Fig. 3. Locations of monitoring sites in East Asia. Gridpoints with emission are labeled '1'. No fraction of land was considered.

and agreed well with the measured concentrations for northern China (Hahehaote, Changchun, Beijing, and Nanjing), but were about half of the measured concentrations for southern China (Xi'an, Wuhan, and Guiyang). Simulated concentrations for the coast (Shanghai, Fuzhou, and Gaoxlong) underestimated the measured concentrations. These stations are located at the edge of the continent or on an island, and have no emissions within their grids (Fig. 3).

Similar to the results for February and November in Freiburg, insufficient vertical resolution in the model is a possible cause for the disagreement at inland stations, although we do not have detailed information about the height of stable layers at night. Therefore, our discussion is confined to maximum mixing depth. Figure 5 is the same as Fig. 2 except that it is for six inland stations in China. Seasonal variation of surface concentration in northern China (Huhehaote, Changchun, Beijing, and Xi'an) might be explained by the seasonal change of MMD. April to June were the months of highest MMD at Huhehaote, Changchun, and Xi'an, and were also the months of minimum concentration. The same trend was seen in April and May at Beijing. Relatively constant simulated surface concentrations at Wuhan and Guiyang are consistent with the constant MMD throughout the year.
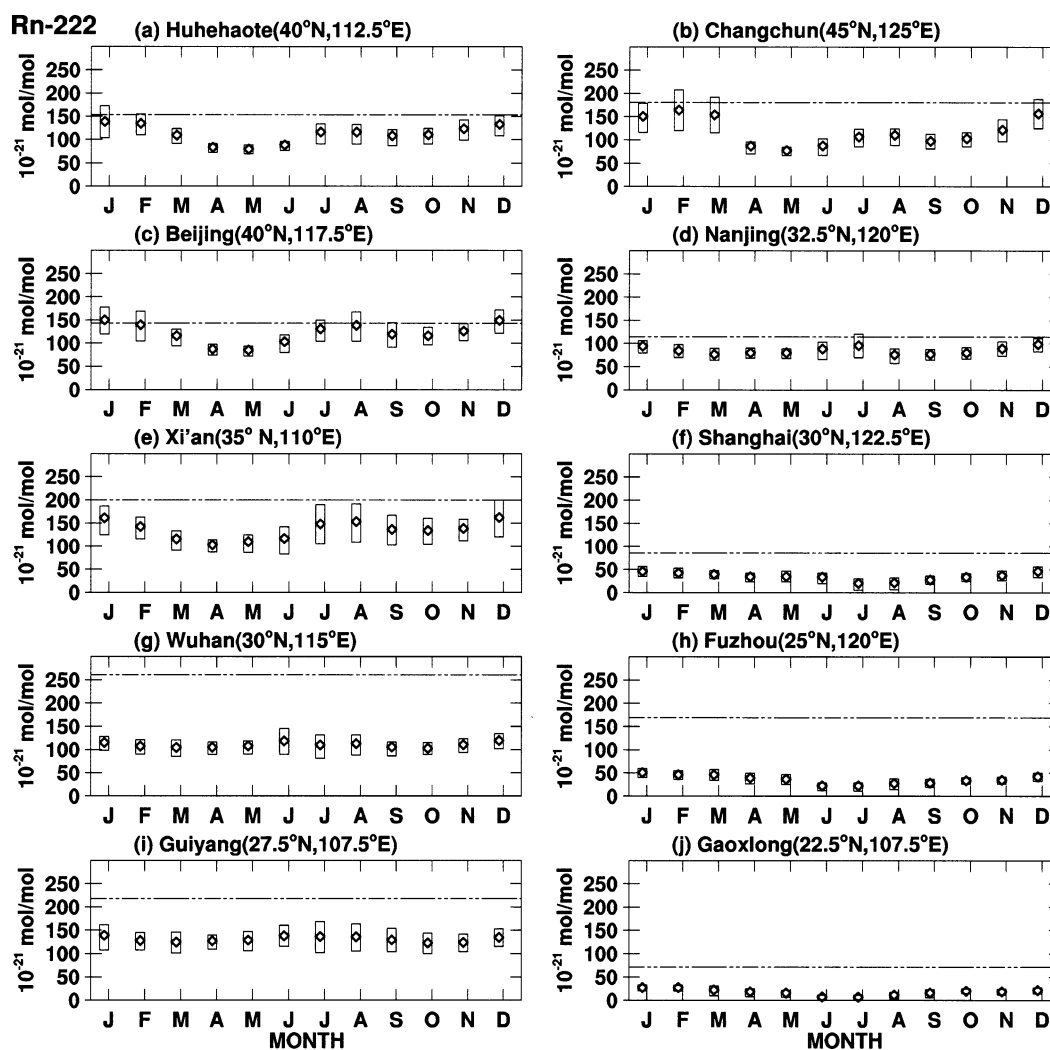
Fig. 4. ^{222}Rn concentrations measured (closed circles) and simulated by using the NIRE-CTM-96 (open circles) for China. Box indicates quartile of daily average of concentration simulated for a 6-yr period, between 1991 and 1996. (a) Huhehaote (40.8°N, 111.7°E), (b) Changchun (43.9°N, 125.2°E), (c) Beijing (39.9°N, 116.3°E), (d) Nanjing (32.0°N, 118.8°E), (e) Xi'an (34.3°N, 108.9°E), (f) Shanghai (31.2°N, 121.4°E), (g) Wuhan (30.6°N, 114.1°E), (h) Fuzhou (26.1°N, 119.3°E), (i) Guiyang (26.6°N, 106.7°E), and (j) Gaoxlong (22.0°N, 120.8°E). Locations of gridpoints where model concentrations were calculated are listed in each panel. Statistics are based on simulations for a 6-yr period (1991–1996). Horizontal lines show mean concentrations for 1989–1990 and 1990–1991 reported by Jin et al. (1998).

We used MMD estimated from radiosonde temperature for validations. Gamo et al. (1993) reported the height of MMD for China for August 1987 (dots in Fig. 5) using a vertical profile of temperature obtained at 8 am Beijing standard time. A range of mixed layer depth was estimated using temperature profile at 2 pm was obtained in May to June, 1998 at Wuhan from Tibetan Plateau Experiment (personal communication with Liu Huizhi, 2001) and was show by arrows. Although

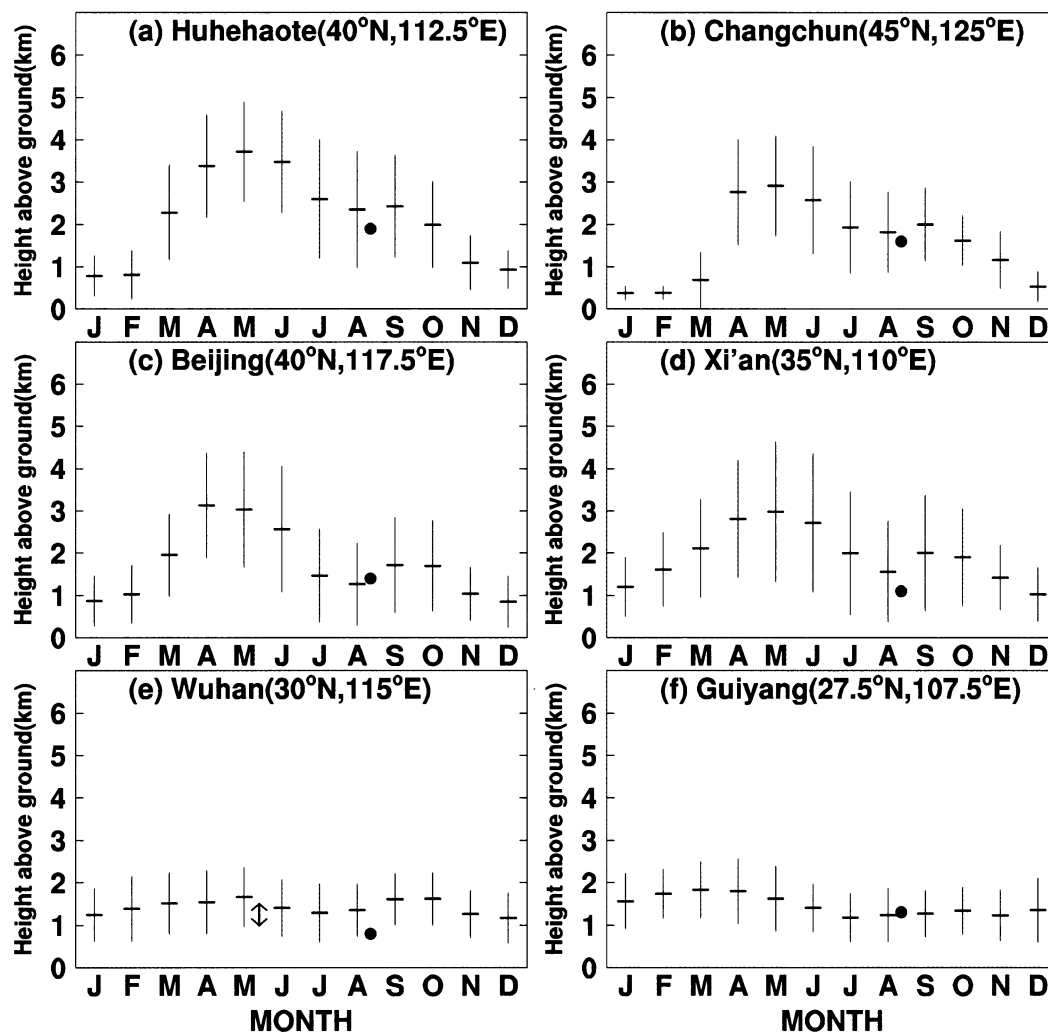## Daily Maximum Thickness of Mixed Layer(km) (1990-1996)

Fig. 5. Daily maximum thickness of well-mixed layer in the model at China. (a) Huhehaote, (b) Changchun, (c) Beijing, (d) Xi'an, (e) Wuhan, and (f) Guiyang. Maximum depth of mixed layer estimated in August 1987 (Gamo, 1993) is indicated by dots. A range of mixed layer depth estimated in May to June 1998 (personal communications with Liu) is shown by arrows.

the agreement of MMD estimated by radiosonde observations was achieved only for limited period, the disagreement between simulated and measured ^{222}Rn concentrations at Wuhan and Guiyang was probably caused by inaccuracy in the emanation rate used in the model rather than by the deficiencies in the MMD.

5. Ogasawara-Hahajima

Temporal aspect of the model behavior was investigated at remote sites south of Japan. Relative contributions to the ^{222}Rn concentrations at these remote stations were studied using tags attached to ^{222}Rn released from the 15 land

sections shown in Fig. 6. Land divisions were based on a vegetation map, and thus were somewhat arbitrary. Nomenclature for each section is shown in the figure caption.

Measurement and simulated concentrations at Ogasawara-Hahajima (26.6°N, 142.2°E) are shown in Fig. 7. Upper panels show the simulated daily average concentrations for selected land sections in 1996 at Ogasawara-Hahajima. The lower panel shows the summation of simulated concentrations (labeled 'NIRE-CTM-96') and measured concentrations (labeled 'OBS') from all land sections. Our model well reproduced the observed seasonal cycles. The correlation coefficient between measured and simulated concentrations was 0.78.

For autumn, winter, and spring, the largest contribution to the ^{222}Rn concentration came from the land area northeast of Hahajima Island (stations 7, 10, 11 shown in Fig. 6). On average, the major portion of ^{222}Rn at Hahajima was transported from Siberia, north of 50°N, and only a small portion was transported from the land area south of Hahajima.

In summer, simulated concentrations indicate that Hahajima was generally covered by maritime air mass. The minimum detectable concentration of the instrument used to measure the ^{222}Rn concentration was 5×10^{-21} mol mol^{-1}. This detection limit might be the reason for an offset concentration of about 5×10^{-21} mol mol^{-1} remaining in the measurement for summer.

Although only qualitative interpretation was possible near this lower limit of the observations, the model indicated two instances of land airmass transport occurring in July and August. In July, the land airmass came from the Korea–Japan area, and on 9 August, it came from the Indonesian archipelago and Australia (labeled 'A' in the figure).

Figure 8 shows the simulated concentrations at the fourth model layer (about 700 hPa) and at the lowest model layer from Australia, revealing a cross-equatorial transport on 9 August 1996. On that day, a typhoon was slowly migrating at 25°N, 132°E, and a low-pressure system was located at 30°N, 150°E. From July to August 1996, the sub-tropical northwest Pacific was covered by active convections. Those convections might be responsible for this cross equatorial transport.

6. Mauna Loa

To investigate the cause of discrepancies between model and observations, at Mauna Loa, time-resolved concentrations were compared. Figure 9 shows time-resolved concentrations at Mauna Loa in February 1993 (a) and July 1993 (b). For comparison with TM3-FG (Dentener et al., 1999), the abscissa is in units of mBq/SCM (10^{-21} mol mol^{-1} = 56 mBq/SCM). Measured concentrations were averaged for each 6-h period to coincide with the simulations. Measured con-
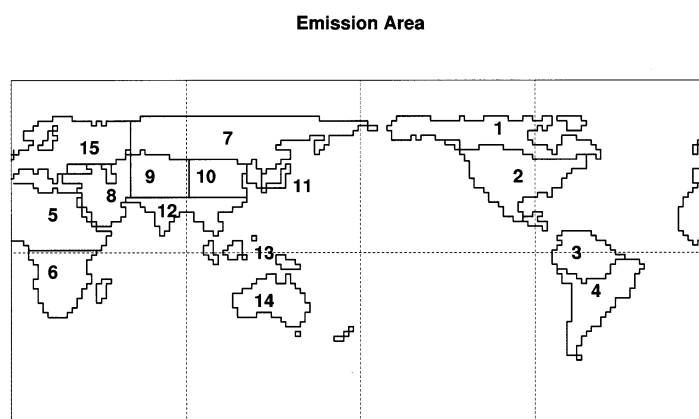
Emission Area

Fig. 6. Emission areas used in the study. (1) Canada, (2) USA, (3) the Amazon, (4) South America, (5) North Africa, (6) South Africa, (7) Siberia, (8) Middle East, (9) Central Eurasia, (10) China, (11) Korea–Japan, (12) India–Indochina, (13) Indonesia, (14) Australia, and (15) Europe.
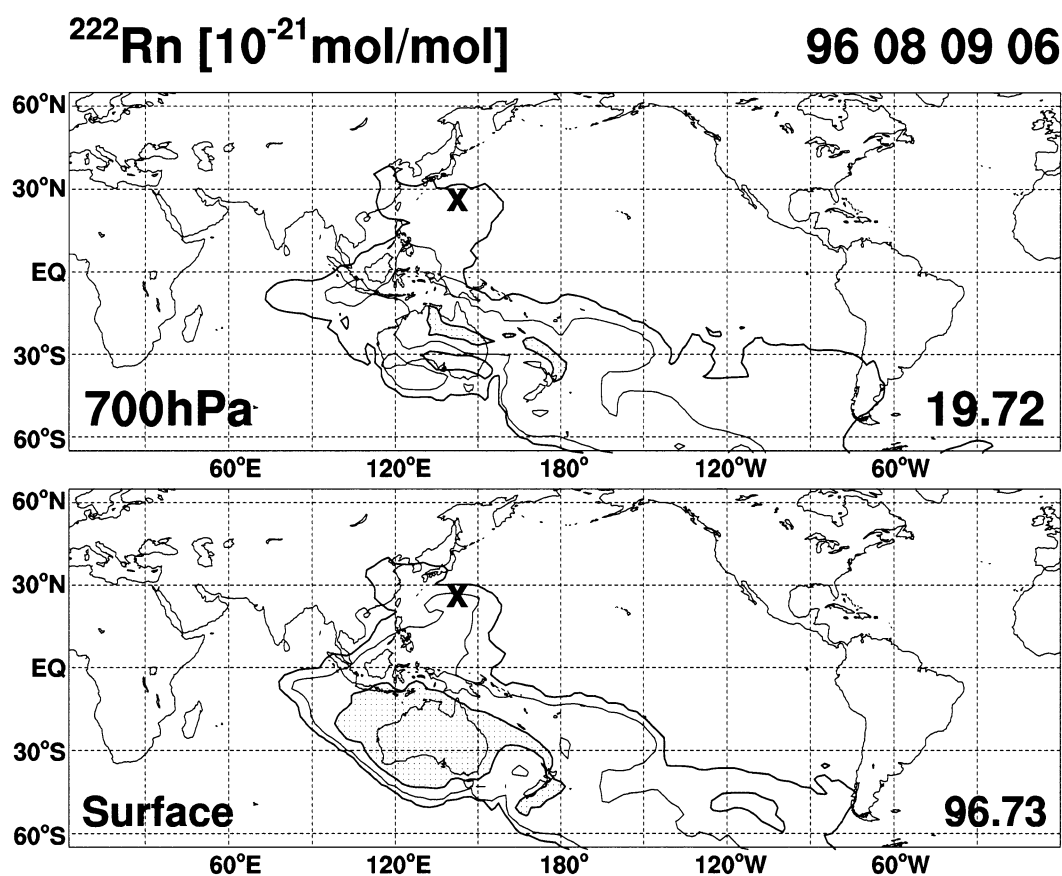
Rn-222 Hahajima (27.5°N 142.5°E)   **1996 Area**

Fig. 7. Simulated daily concentrations for Hahajima in 1996. The upper five panels show the concentrations transported from Siberia (7 in Fig. 6), China (10), Korea–Japan (11), Indonesia (13), Australia (14) and the sixth panel shows the total concentration from remaining land sections. The lower figure shows the total contributions from land and the measured concentrations. The event labeled 'A' is discussed in the text.

centrations that we used in the comparison differed slightly from those shown by Dentener et al. (1999) probably because the data file we acquired in January 2001 was updated from the data file used by Dentener et al. (1999) (personal communication with Lee, 2001). The figure also shows the simulated concentrations added to the possible contributions $(0.5 \times 10^{-21} \, \text{mol mol}^{-1})$ from oceanic emissions of 0.01 atom cm^{-2} s^{-1}.

In February 1993, five radonic storms that lasted less than 3 d might be subjectively defined

as occurring on Julian days 45, 48, 52. None of them was reproduced by the model. The storm occurring on day 52 (21 February, marked 'I') will be decomposed by land sections later in this section. In July 1993 (Julian days 180–213, Fig. 9b), fluctuations in the measured concentrations were less than those in other months. On Julian day 200 (marked 'C'), measured concentration was low, whereas simulated concentration was high.

Figure 10 shows time-resolved concentrations

222Rn [10^-21 mol/mol]   96 08 09 06

Fig. 8. Cross-equatorial transport from Australia (area number 14 in Fig. 6). Instantaneous concentrations at 6 UTC 9 August 1996 at the fourth model level (about 700 hPa) (top) and the lowest sigma level (bottom). The location of Hahajima is indicated by ×. Contours are 0.1, 1, 10, and 100×10^{-21} mol mol^{-1}.

for Mauna Loa simulated by using seven selected land sections. The sharp increase in February (labeled 'I' in the figure) is possibly related to transport from the India–Indochina area. Transport from Siberia (area 7 in Fig. 6) was observed prior to the increase I and another transport from USA (area 2) after the increase I. We could eliminate the possibility that local sources from the island of Hawaii produced the sharp peak because transport from remote islands was active. Failure of the model to simulate this peak (Fig. 9) was assumed to be related to incorrect modeling of the transport from the India–Indochina area.

Figure 11 shows simulated concentrations of ^{222}Rn on 21 February 1993 at 300 (top) and

700 hPa (bottom) released from the India–Indochina area. Mauna Loa is indicated by a cross on the map. The axis of high concentration passed by at 10°N of Mauna Loa at both 300 and 700 hPa. Note that concentrations are higher in the upper troposphere than those in the lower troposphere over the north Pacific Ocean for this tracer, which demonstrates the results of fast advective transport in the upper troposphere.

To obtain an accurate concentration by using the model, we asked six questions. First, is there a failure in accurately positioning the axis of the above-mentioned high concentration? If we assume that positioning error occurred randomly, then systematic underestimation cannot be explained. Because we currently have no informa-
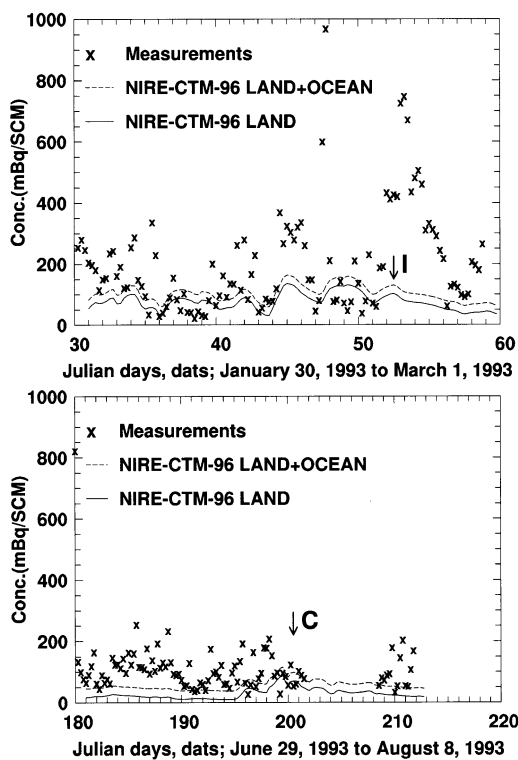
Fig. 9. Time-resolved concentrations for Mauna Loa for February (a) and July (b) 1993, showing measured concentration (*x*), simulated concentration from land source only (solid line), and from land and oceanic sources combined (dashed line).

tion regarding horizontal distribution of ^{222}Rn, resolving this issue of positioning error must wait until such information is available.

Second, is there any missing axis of high concentration? This might be possible if we missed a convection that was not represented in the meteorological data. However, to find any source of ^{222}Rn for the 700 hPa level by convection unresolved in the $2.5° \times 2.5°$ resolution data, requires an extensive survey of satellite images, and thus is beyond the scope of the present study. Third, are there any missing structures unresolved in the $2.5° \times 2.5°$ resolution model? Although Dentener et al. (1999) discussed the effect of horizontal resolution of the model using different grid spacings from $7.5° \times 10°$ to $2.5° \times 2.5°$, they did not discuss the fine structure of the tracer distributions smaller than the horizontal resolution of the model. Waugh and Plumb (1994) discussed a

horizontal fine structure and showed that horizontal atmospheric transport inherently produces a streak of tracer at the hemispheric scale. They called such a streak a 'filament'. An airmass of high ^{222}Rn concentration might have a horizontal scale of 860 km if it is transported with a typical wind speed at 700 hPa at 20°N 155°W, 10 m s^{-1}, and is observed for one day. The model CTM with 2.5° resolution (about 250 km) does not have ability to simulate horizontal distribution of 860 km width. Fifth, is it possible to simulate the fine structure using an existing advection scheme or convective parameterization? A slope scheme (Russel and Lerner, 1981) was used in TM3, and a semi-Lagrangian transport scheme with shape-preserving interpolation (Rasch and Williumson, 1990) was used in ECHAM. Furthermore, TM3-FG and ECHAM use Tiedke's cloud flux scheme (Tiedke, 1989), whereas our model uses no moist convective transport. Nevertheless, Dentener et al. (1999) showed that TM3-FG and ECHAM underestimated concentrations at Mauna Loa. Therefore, use of either a slope method, a semi-Lagrange method with shape-preserving interpolation, or cloud flux parameterization will probably not eliminate this problem of the model not representing the fine structure. Sixth, is the assumed emanation rate for Eurasia accurate? We tested the possibility of a high emanation rate for Asia, as was done by Dentener et al. (1999). Based on a simple parameter-fitting between simulated and measured daily concentrations, we found that the agreement could be improved by increasing the emanation rate used in our simulation by a factor of more than 5, depending on the year of the measurement and on the site. For example, agreement was improved by increasing the emanation rate for southern China by a factor of 2 (2 atom cm^{-2} s^{-1}) based on the simulation at Wuhan (Fig. 4g). No such factor was needed for Europe or India, based on Freiburg (Fig. 1a) and Bombay (Fig. 1d), respectively. Although enhancement in the emanation rate for Eurasia actually improved the agreement, doubling the emanation rate does not completely explain the discrepancy between simulation and the observation.

Figure 12 shows simulated transport from Canada on 19 July 1993. Southward flow in summer from North America was a significant part of ^{222}Rn at Mauna Loa. This transport was
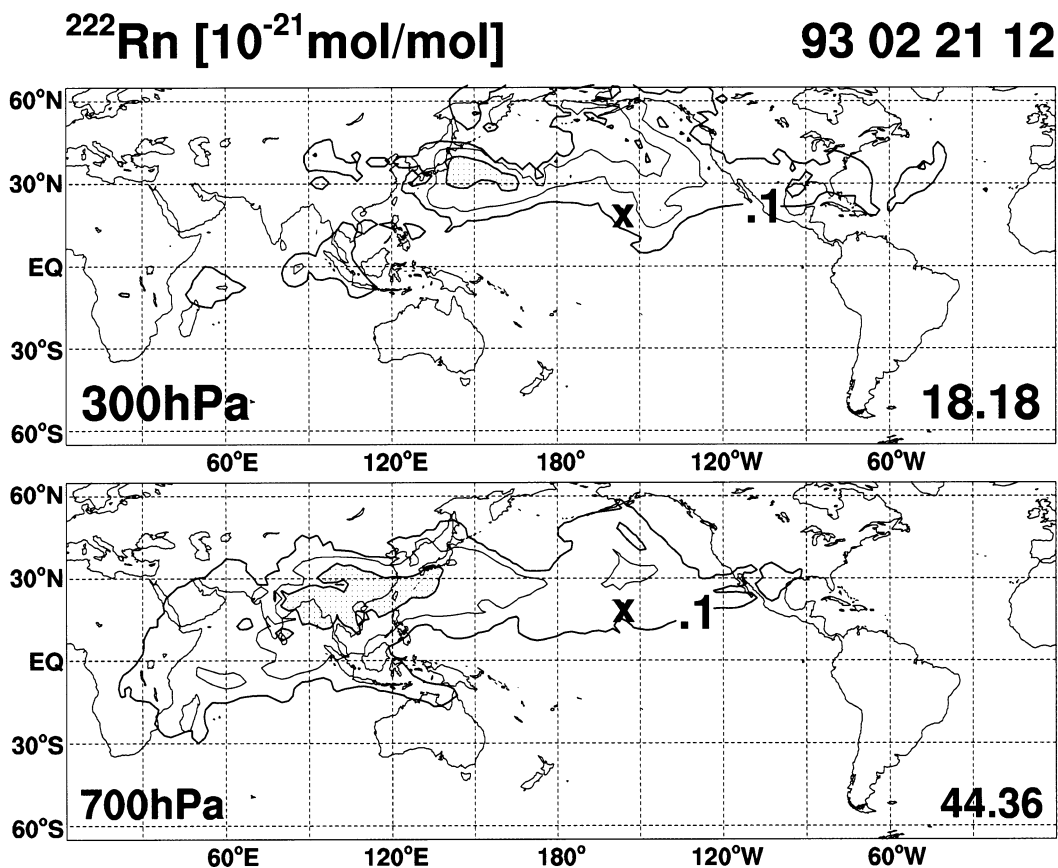
Fig. 10. Simulated concentrations for Mauna Loa in 1993 from seven selected land sections: Canada (1 in Fig. 6), USA (2), Siberia (7), Central Asia (9), China (10), Korea–Japan (11), and India–Indochina (12). Events labeled 'I' and 'C' are identical to those in Fig. 9.

larger at lower levels than at the middle troposphere, counter to the transport from the India–Indochina area. Although, no information about the source of high concentration prior to event 'C' is available, simulated concentrations agreed with the measured concentrations (Fig. 9).

7. Moffet field

The last aspect of the model that we explored in our evaluation was vertical distribution. Vertical distributions of ^{222}Rn at Moffet Field, California, USA, were measured by Kritz et al. (1998). By using the measurements at Moffet Field, Stockwell et al. (1998) validated a chemical transport model (TOMCAT) developed at the University of Cambridge. Figure 13 shows measured and simulated vertical distributions of ^{222}Rn for selected sections, Canada (1 in Fig. 3), the USA (2), Central Eurasia (9), China (10), and the India–Indochina area (12). Simulated vertical profiles were taken at 122.5°W, 37.5°N, although measurements were

Fig. 11. Instantaneous concentrations on 21 February 1993 for India–Indochina. The 300 hPa (top) and the fourth model level (about 700 hPa) (bottom). The location of Mauna Loa is indicated by ×. Contours are 0.1, 1, 10, and 100×10^{-21} mol mol^{-1}.

taken within a 10-degree area around this point. Details of sampling locations were described in Kritz et al. (1998).

On 7 June 1994, simulated concentrations at altitudes above 4 km were larger than those below 4 km, and the largest contributions to the upper tropospheric concentrations came from Central Eurasia and China. On 14 June 1994, the largest contributions came from the India–Indochina area and China. For both days, at altitudes above 8 km, the simulation indicated that areas outside of China contributed more than did China itself. A long-distance rapid transport, denoted as the 'China Clipper' (Kritz et al., 1990), is a caveat when using a regional model to interpret the tracer distribution. ^{222}Rn from Canada (1) and the

USA (2) are dominant contributors only to the lower part of the troposphere below 2 km.

Simulated vertical profiles have less vertical structure than do observed profiles. The laminated structure of atmospheric traces was demonstrated by Stoller et al. (1999) based on O_3, CO, CH_4 and H_2O observations (by using aircraft) over the Pacific Ocean. Stoller et al. (1999) estimated the density of the layers as 0.29 layers per km in the north Pacific (PEM-West A). Vertical scale of layers was on the order of 1 km. The lack of vertical structure in the simulation is another possible reasons, other than six issues raised in the previous section, for failure to simulate accurately the high concentration peak at Mauna Loa in the model.
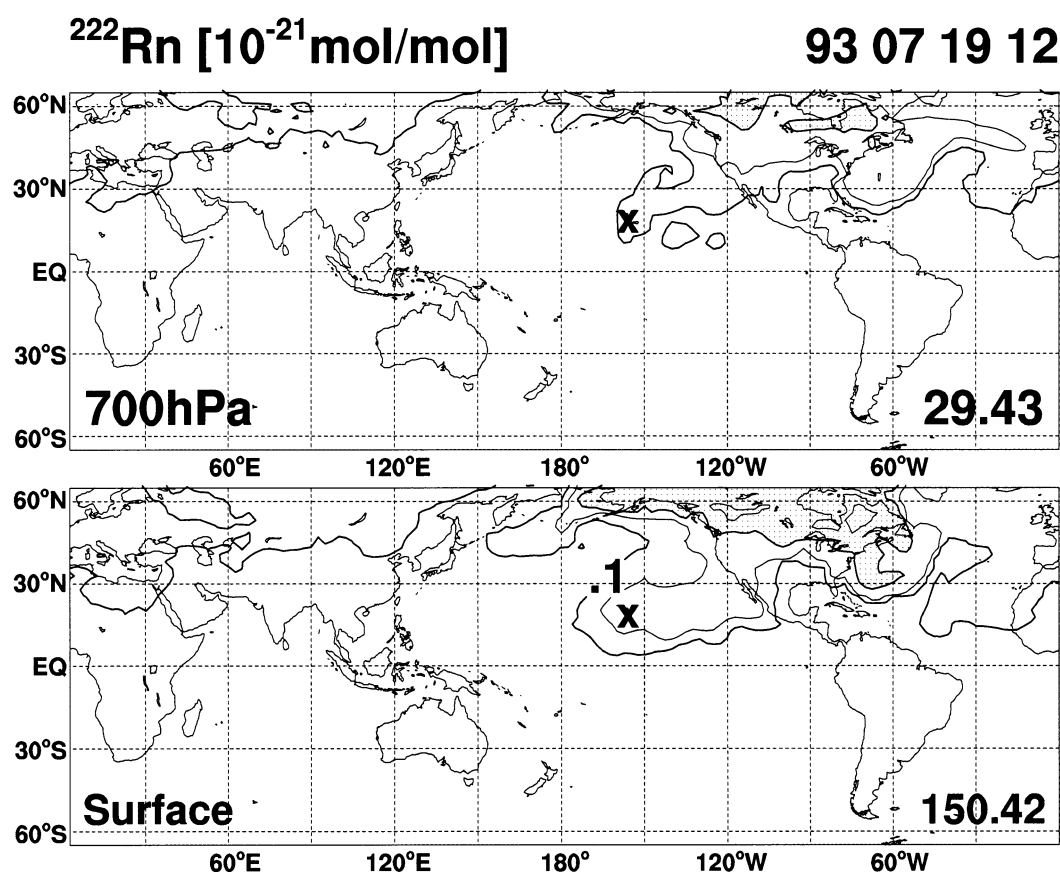
Fig. 12. Instantaneous concentrations on 16 July 1993 for Canada. The continental outflow from North America to subtropical north Pacific were observed. Contours are 0.1, 1, 10, and 100×10^{-21} mol mol^{-1}.

8. Conclusions

A global chemical transport model, NIRE-CTM-96, was tested using ^{222}Rn. NIRE-CTM-96 reproduced the measured concentrations of ^{222}Rn at 17 of 22 monitoring stations if we used an emanation rate of ^{222}Rn from land of 1 atom cm^{-2} s^{-1} and from oceanic sources of 0.01 atom cm^{-2} s^{-1}. Emanation from oceans was a significant part of the concentrations at remote sites in the South Indian Ocean and the Antarctic in summer. The model indicated higher rates of emanation in the range 1.5–2 in southern China. The model underestimated the concentrations at inland stations in winter, probably due to insufficient vertical resolution of the model near the surface. Time-resolved measurement of mixed layer depth and ^{222}Rn concentrations at inland

stations might help determine the contribution of nocturnal high concentrations to mean concentrations. Mixed layer depth in the model in the spring was suggested to be thicker than the actual mixed layer over high terrains. The model failed to reproduce a sharp increase in concentration at Mauna Loa. Possible reasons for this failure include numerical diffusion of filamentation of high-concentration areas, or insufficient vertical resolution of the model to keep laminated layers. The only way to confirm these reasons is to develop a fine-resolution model. Due to the limited ability of the transport model NIRE-CTM-96, measurements of ^{222}Rn concentrations measured during an aircraft campaign provide an excellent tag for airmass recently mixed with air in the surface boundary layer over land, especially when the airmass is forming a filament or lamination.
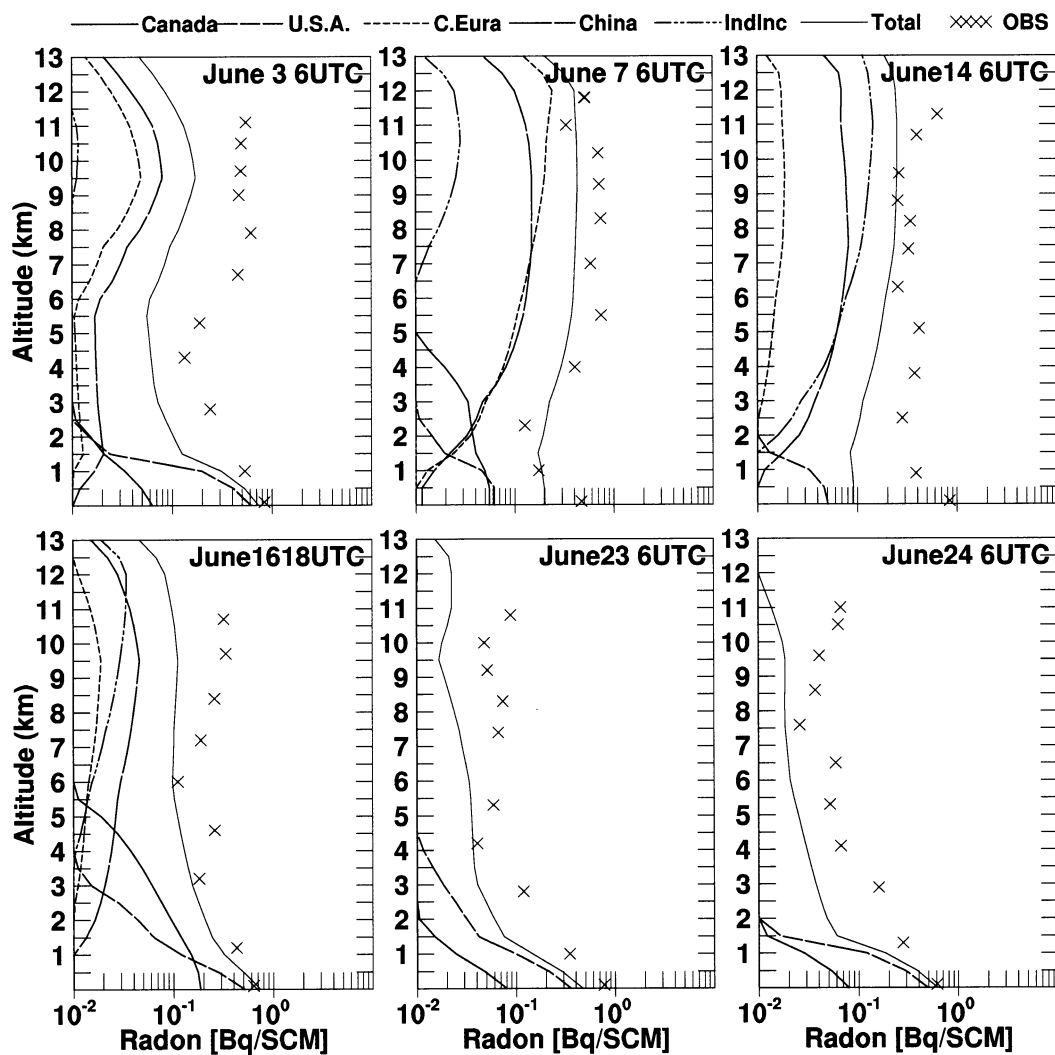
Fig. 13. Moffet Field measured profile (×) and the NIRE integrations for total area and some selected sections: Canada (1 in Fig. 6), USA (2), Central Eurasia (9), China (10), and India–Indochina (12). Contributions from other sections were insignificant. All model vertical profiles were taken from 37.5°N, 122.5°W.

REFERENCES

Brasseur, G. P., Hauglustaine, D. A., Walters, S., Rasch, P. J., Müller, J.-F., Granier, C. and Tie, X. X. 1998. MOZART, a global chemical transport model for ozone and related chemical tracers. 1. Model description. *J. Geophys. Res.* **103**, 28,265–28,289.

Denning, A. S., Holzer, M., Gurney, K. R., Heimann, M., Law, R. M., Rayner, P. J., Fung, I. Y., Fan, S.-M., Taguchi, S., Friendlingstein, P., Balkanski, Y., Taylor, J., Maiss, M. and Levin, I. 1999. Three-dimensional transport and concentration of SF$_6$, a model intercomparison (TransCom 2). *Tellus* **51B**, 266–297.

Dentener, F., Feichter, J. and Jeuken, A. 1999. Simulation of the transport of ^{222}Rn using on-line and off-line global models at different horizontal resolutions: A detailed comparison study with measurements. *Tellus* **51B**, 573–602.

Feichter, J. and Crutzen, P. J. 1990. Parameterization of vertical tracer transport due to deep cumulus convection in a global transport model and its evaluation with ^{222}Rn measurements. *Tellus* **42B**, 100–117.

Gamo, M., Hayashi, M., Tamagawa, I. and Mitsuya, Y. 1993. Seasonal variations of the mixed layer characteristics in the HEIFE area. *Proceedings of International Symposium on HEIFE*. Disaster Prevention Research Institute, Kyoto University and Lanzhou Institute of Plateau Atmospheric Physics, CAS, 316–321.

Genthon, C. and Armengaud, A. 1995. Radon-222 as a comparative tracer of transport and mixing in two general circulation models of the atmosphere. *J. Geophys. Res.* **100**, 2849–2866.

Gesell, T. F. 1983. Background atmospheric ^{222}Rn concentrations outdoors and indoors: a review. *Health Phys.* **45**, 289–302.

Heimann, M. and Keeling, C. 1989. A three-dimensional model of atmospheric CO$_2$ transport based on observed winds: 2. Model description and simulated tracer experiments. *Geophys. Monogr.* (ed. D. H. Peterson), vol. 55. American Geophysical Union, Washington D.C., USA, 237–275.

Hoinka, K. P. 1998. Statistics of the global tropopause pressure. *Mon. Wea. Rev.* **126**, 3303–3325.

Jacob, D. J. and Prather, M. J. 1990. Radon-222 as a test of convective transport in a general circulation model. *Tellus* **42B**, 118–134.

Jacob, D. J., Prather, M. J., Rasch, P. J., Shia, R.-L., Balkanski, Y. J. and coauthors, 1997. Evaluation and intercomparison of global atmospheric transport models using ^{222}Rn and other short-lived tracers. *J. Geophys. Res.* **102**, 5953–5970.

Jin, Y., Iida, T. Wang, Y. I. Z. and Abe, S. 1998. A subnationwide survey of outdoor and indoor ^{222}Rn concentrations in China by passive method. *Radon and thoron in the human environment. Proceedings of the 7th Tohwa University International Symposium* (eds.

A. Katase and M. Shimo). World Scientific, Singapore, 276–281.

Kritz, M. A., Rosner, S. W. and Stockwell, D. Z. 1998. Validation of an off-line three-dimensional chemical transport model using observed radon profiles, 1. observations. *J. Geophys. Res.* **103**, 8425–8432.

Kritz, M. A., Le Roulley, J.-C. and Danielsen, E. F. 1990. The China clipper — fast advective transport of radon-rich air from the Asian boundary layer to the upper troposphere near California. *Tellus* **42B**, 46–61.

Lambert, G., Polian, G. and Taupin, D. 1970. Existence of periodicity in Radon concentration and in the large-scale circulation at lower altitudes between 40° and 70° south. *J. Geophys. Res.* **75**, 2341–2345.

Law, R. M., Rayner, P. J., Denning, A. S., Erickson, D., Heimann, M., Piper, S. C., Ramonet, M., Taguchi, S. Taylor, J. A., Trudinger, C. M. and Watterson, I. G. 1996. Variations in modelled atmospheric transport of carbon dioxide and the consequences for CO$_2$ inversions. *Global Biogeochem.* **10**, 783–796.

Lindeken, C. L. 1966. Seasonal variations in the concentration of airborne radon and thoron daughters. *USAEC Rep. UCRL-50007*. University of California Lawrence Radiation Laboratory, Livermore, CA, 41–43.

Mahowald, N. M., Rasch, P. J., Whittlestone, S. and Prinn, R. G. 1997. Transport of radon-222 to remote troposphere using the model of atmospheric transport and chemistry and assimilated winds from ECMWF and the National Centre for Environmental Predictions/NCAR. *J. Geophys. Res.* **102**, 28,139–28,151.

Mishra, U. C., Rangarajan, C., and Eapen, C. D. 1980. Natural radioactivity of the atmosphere over the Indian land mass, inside deep mines, and over adjoining oceans. *Natural Radiation Environment III, US Department of Energy, Special Symposium Series 51, CONF 780422*. US Department of Energy, Washington, DC, 327–346.

Moore, H. E., Poet, S. E. and Martell, E. A. 1973. ^{222}Rn, ^{210}Po, ^{210}Bi, and ^{210}PO profiles and aerosol residence times versus altitude. *J. Geophys. Res.* **78**, 7065–7075.

Ramonet, M., Le Roulley, J. C., Bousquet, P. and Monfray, P. 1996, Radon-222 measurements during the Tropoz II campaign and comparison with a global atmospheric transport model. *J. Atmos. Chem.* **23**, 107–136.

Rasch, P. and Williumson, D. 1990. On shape preserving interpolation and semi-Lagrangian transport. *SIAM J. Sci., Stat. Comput.* **11**, 656–687.

Russel, G. L. and Lerner, J. A. 1981. A new finite-differencing scheme for the tracer transport equation. *J. Appl. Meteorol.* **20**, 1483–1498.

Schery, S. D. and Wasiolek, M. A. 1998. Modeling radon flux from the earth's surface. *Radon and Thoron in the human environment, Proceedings of the 7th Tohwa Uni-*

versity International Symposium (eds. A. Katase and M. Shimo). World Scientific, Singapore, 207–217.

Stockwell, D. Z., Kritz, M. A., Chipperfield, M. P. and Pyle, J. A. 1998. Validation of an off-line three-dimensional chemical transport model using observed radon profiles, 2. Model results. *J. Geophys. Res.* **103**, 8433–8445.

Stoller, P., Cho, J. Y. N., Newell, R. E., Thouret, V., Zhu, Y., Carroll, M. A., Albercook, G. M., Anderson, B. E., Barrick, J. D. W., Browell, E. V., Gregory, G. L., Sachse, G. W., Vay, S., Bradshaw, J. D. and Dandholm, S. 1999. Measurements of atmospheric layers from the NASA DC-8 and P-3B aircraft during PEM-Tropics A. *J. Geophys. Res.* **104**, 5745–5764.

Taguchi, S. 1996. A three-dimensional model of atmospheric CO_2 transport based on analyzed winds: model description and simulation results for TRANSCOM. *J. Geophys. Res.* **101**, 15,099–15,109.

Taguchi, S., Matsueda, H., Inoue, H. Y. and Sawa, Y. 2002. Long-range transport of CO from tropical ground to upper troposphere: A case study for South East Asia in October 1997. *Tellus* **54B**, 22–4.

Tiedtke, M. 1989. A comprehensive mass flux scheme for cumulus parametrization in large-scale models. *Mon. Wea. Rev.* **117**, 1779–1800.

Troen, I. and Mahrt, L. 1986. A simple model of the atomospheric boundary layer; senstivity to surface evaporation. *Boundary-Layer Meterol.* **37**, 129–148.

Turekian, K. K., Nozaki, Y. and Benninger, L. K. 1977. Geochemistry of atmospheric radon and radon products. *Ann. Rev. Earth Planet. Sci.* **5**, 227–255.

Waugh, D. and Plumb, R. A. 1994. Contour advection with surgery: a technique for investigating finescale structure in tracer transport. *J. Atmos. Res.* **51**, 530–540.

Wilkening, M. H. 1959. Daily and annual courses of natural atmospheric radioactivity. *J. Geophys. Res.* **64**, 521–526.